Phase gradient microscopy in thick tissue with oblique back-illumination
Tim N Ford, Kengyeh K Chu & Jerome Mertz

Supplementary Figure 1: Comparison of added versus subtracted raw OBM images

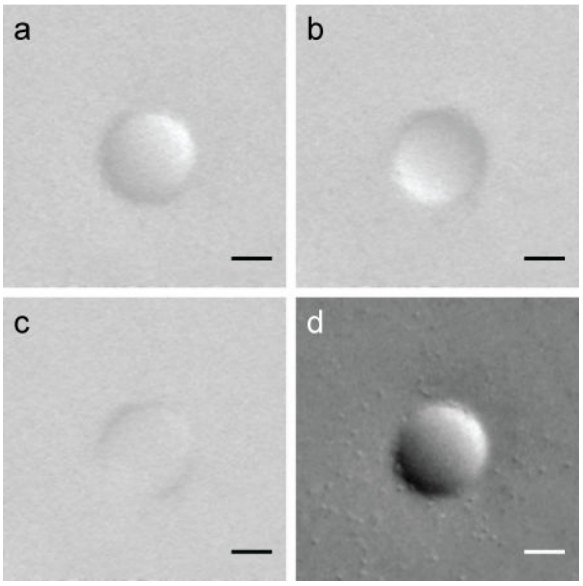

45 μm polystyrene bead embedded in scattering tissue phantom. (**a,b**) raw images under oblique back-illumination from two opposing directions. (**c**) Addition of (**a**) and (**b**) cancels phase gradient contrast and emphasizes absorption. (**d**) Subtraction of (**a**) and (**b**) cancels absorption contrast and emphasizes phase gradients. The 2 μm beads used to render the tissue phantom scattering are readily visible only when in focus. Lateral resolution is ~2.6 μm, limited by the fiber core spacing of the imaging fiber bundle. Scale bars 20 μm.

Supplementary Figure 2: Axial response measured with polystyrene bead tissue phantom

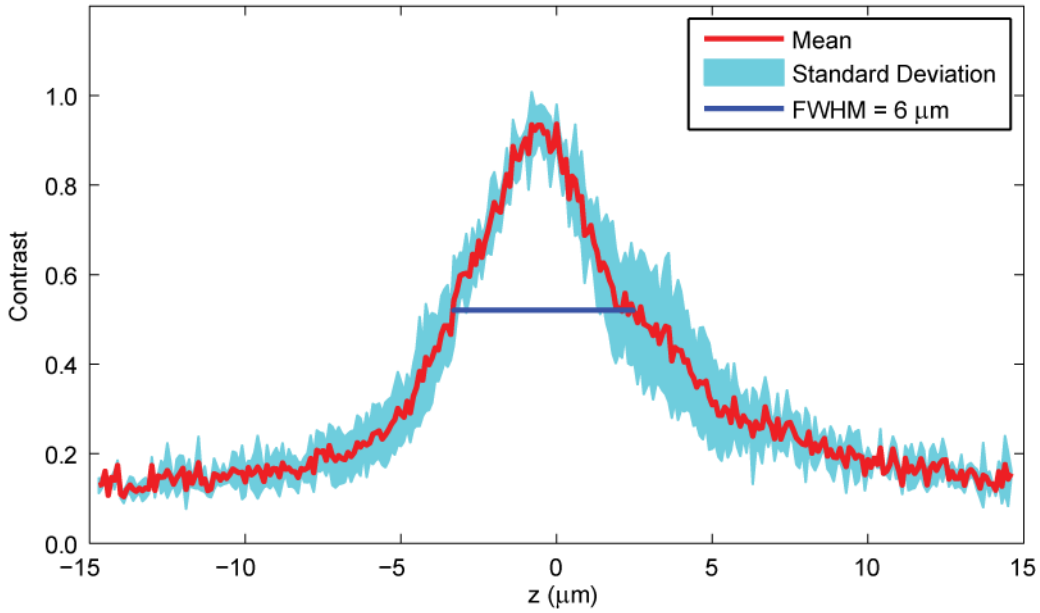

Characterization of apparent OBM axial resolution. A z-stack of OBM phase gradient images was acquired by axially translating a scattering tissue phantom (Online Methods) with a step size ~100 nm. The contrast of five 5.5 × 5.5 μm (12 × 12 pixel) regions each bounding single 2 μm diameter beads was computed as (max – min) / (max + min) for every frame in the z-stack. The resulting contrast profiles were normalized and co-registered. Increasing z corresponds to deeper imaging.

Supplementary Figure 3: OBM depth penetration in mouse brain slice

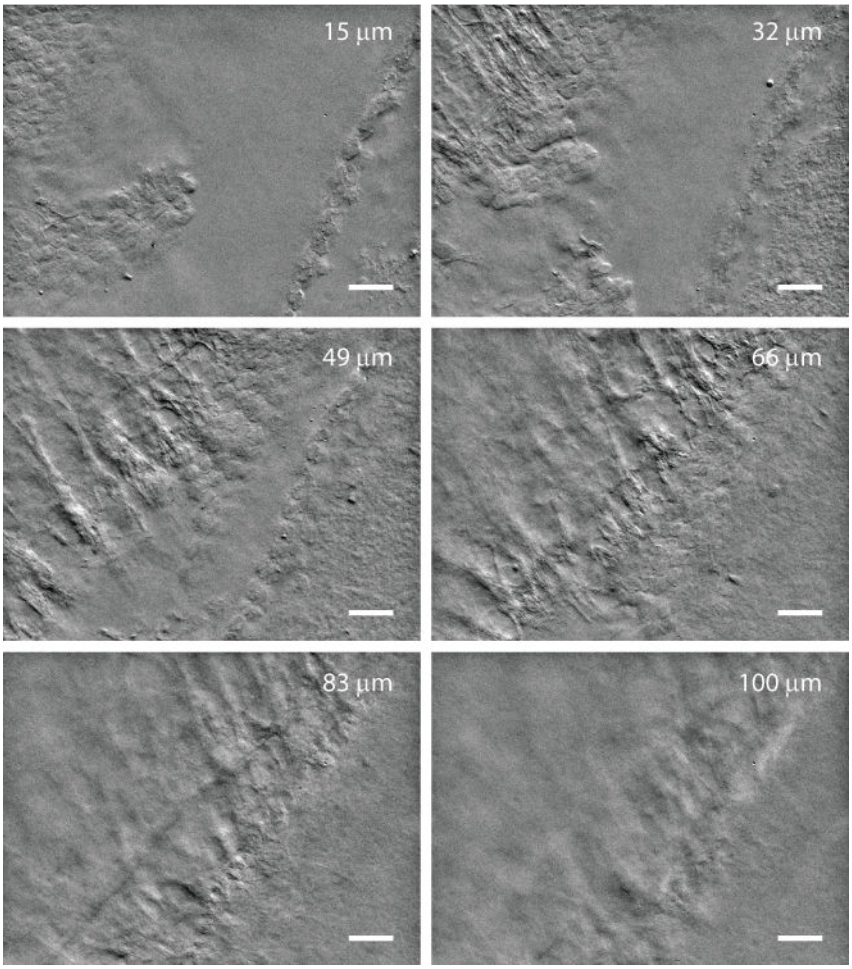

To illustrate OBM penetration depth, the micro-objective and flexible fiber bundle were replaced with a traditional microscope objective (Olympus 40× water immersion, 0.80 NA, working distance 3.3 mm). The two illuminating fibers were guided along the objective housing and placed in contact with the sample. The separation between fiber and objective axes was 4.3 mm. A z-stack of a fixed mouse brain slice (sagittal cut through the brain mid-line) illustrates imaging to a depth of 100 μm, beyond which OBM contrast became too weak to reveal structure. In addition to providing greater working distance, the microscope setup afforded improved spatial resolution (~700 nm, camera pixel limited) compared to the flexible fiber bundle system. Scale bar 30 μm.

Supplementary Figure 4: OBM depth penetration in mouse ventral skin

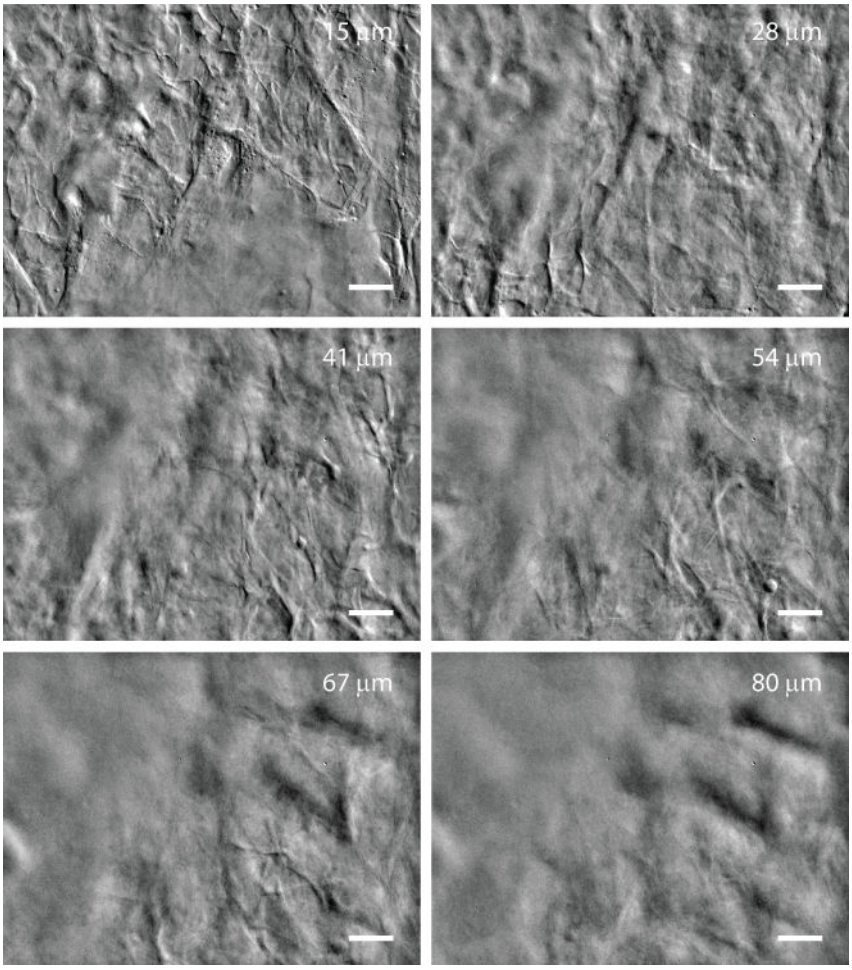

To illustrate penetration depth, OBM was configured in a microscope setup as described in **Supplementary Fig. 3**. A z-stack of fixed mouse ventral skin shows keratin filaments in the stratum corneum down to 80 µm, where the deeper layer of stratum granulosum becomes apparent. Scale bar 30 µm.

Supplementary Figure 5: Comparison of OBM with epi-illumination reflection contrast

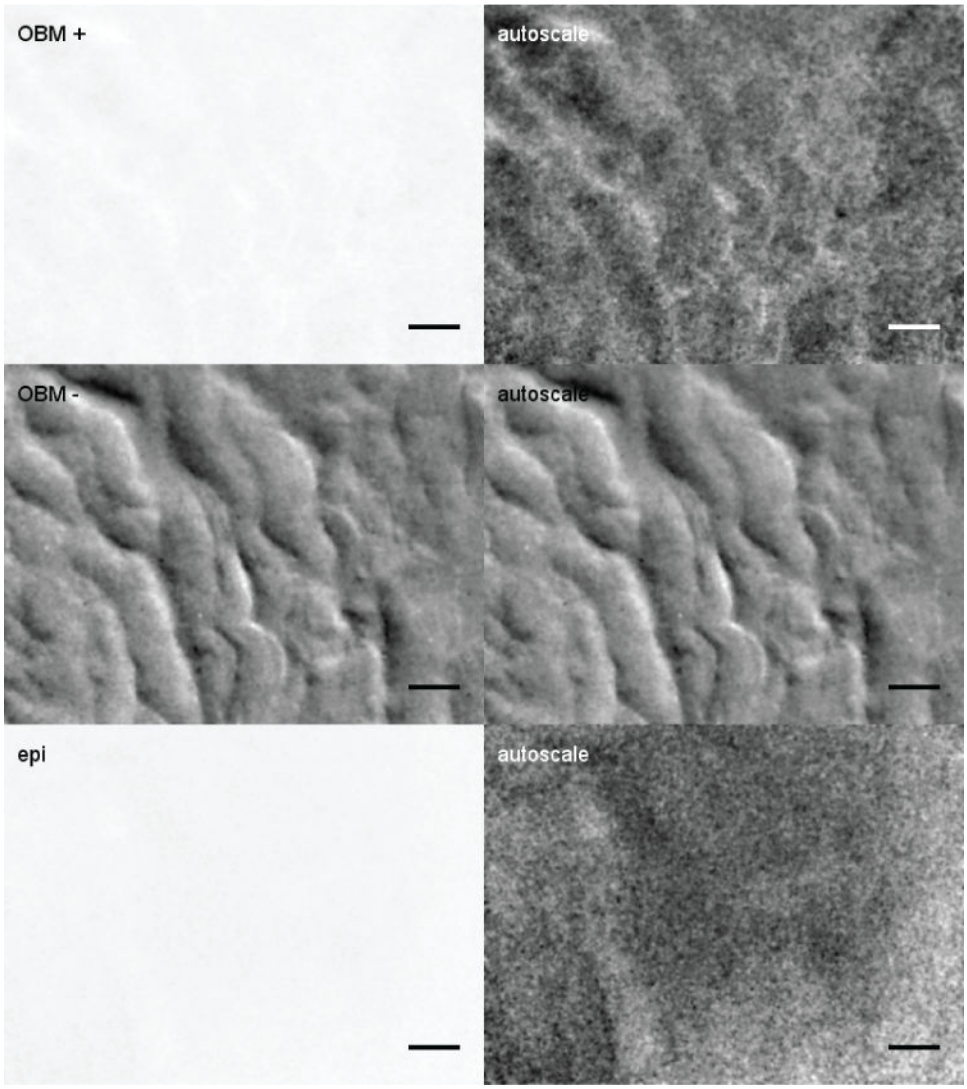

Comparison of OBM and traditional epi-illumination reflection contrast. In the latter case, illumination was delivered to the sample directly through the fiber bundle rather than through separate illumination fibers. To minimize extraneous back reflections from the fiber bundle surface, the illumination and detection paths were cross-polarized. The sample was fixed mouse cardiac muscle tissue. The phase gradient image (OBM –) exhibits significantly higher contrast than either the absorption image (OBM +) or reflection image (epi). The left panels are displayed with the linear grayscale described in the Online Methods. The right panels have been autoscaled

by subtracting the minimum values before scaling up to fill the dynamic range of the display, bringing the contrast of the images to 100%. Note that while the removal of the large biases in the absorption and reflection images improves contrast, signal-to-noise ratio remains too low to reveal meaningful structure. Scale bar 20 μm.

Supplementary Figure 6: Photon exit angle distribution estimated with Monte Carlo simulation

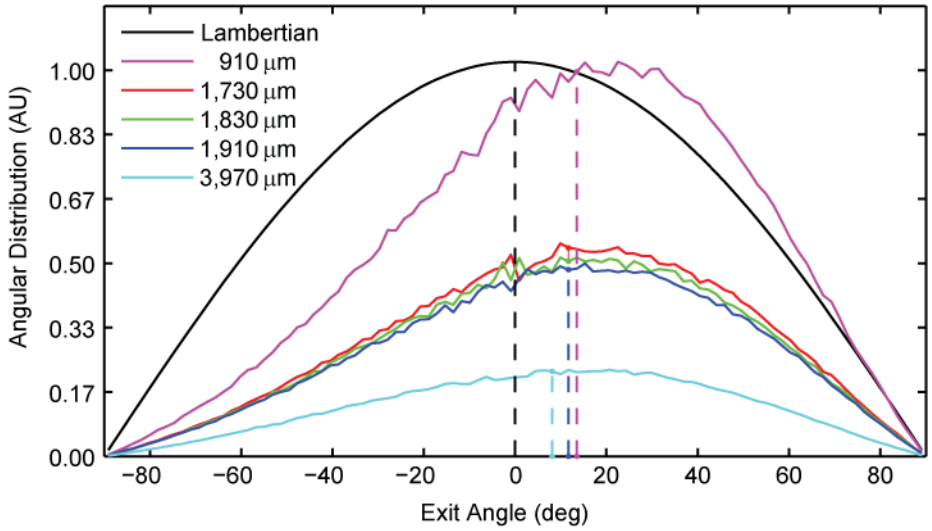

Monte Carlo simulations estimate photon exit angle distributions at different fiber-detector separations. The exit angle corresponds to the tilt angle of the detected photon's path relative to the micro-objective optical axis (positive angles point away from the source). Five fiber-probe separations were considered: 1,830, 1,730 and 1,910 μm correspond to the middle, left, and right extremes of the 2.5× micro-objective FOV, respectively, while 910 and 3,970 μm correspond to roughly half and twice these distances, respectively. The median exit angle for each distribution is noted with a dashed line. A Lambertian exit angle distribution, as would be obtained from isotropic diffuse light in the sample, is also shown for comparison.

Supplementary Figure 7: Exit angle and intensity dependence on fiber-detector separation

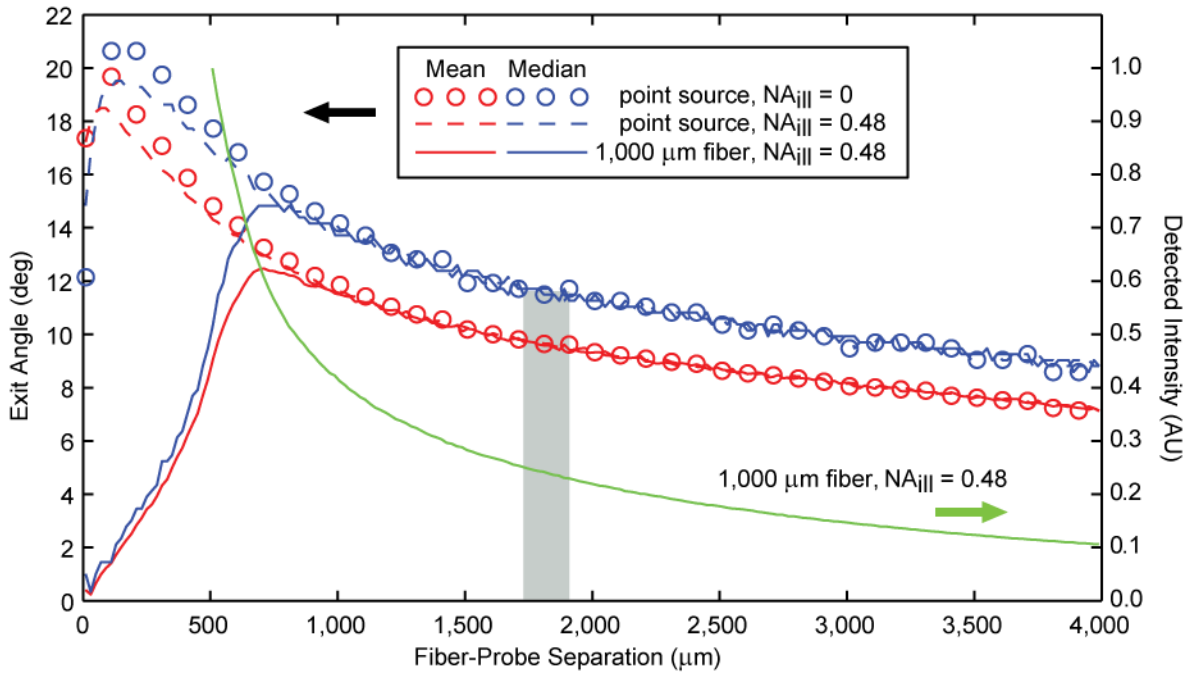

Monte Carlo simulations estimate the dependence of mean and median exit angles and detected intensity as a function of fiber-probe separation. The exit angle corresponds to the tilt angle of the detected photon's path relative to the micro-objective optical axis. The detected intensity is integrated over all exit angles. Three illumination conditions were simulated: a point-source with zero illumination NA, a point source with 0.48 NA, and a 1,000 µm diameter illumination fiber with 0.48 NA. The shaded band represents the actual fiber-probe separation range used in our experiment with the 2.5× micro-objective (FOV = 240 µm).